Single Particle X-ray Diffractive Imaging

M. J. Bogan, W. H. Benner, S. Boutet, U. Rohner, M. Frank, M. Seibert, F. Maia, A. Barty, S. Bajt, V. Riot, B. Woods, S. Marchesini, S. P. Hau-Riege, M. Svenda, E. Marklund, E. Spiller, J. Hajdu, H. N. Chapman

Disclaimer

This document was prepared as an account of work sponsored by an agency of the United States government. Neither the United States government nor Lawrence Livermore National Security, LLC, nor any of their employees makes any warranty, expressed or implied, or assumes any legal liability or responsibility for the accuracy, completeness, or usefulness of any information, apparatus, product, or process disclosed, or represents that its use would not infringe privately owned rights. Reference herein to any specific commercial product, process, or service by trade name, trademark, manufacturer, or otherwise does not necessarily constitute or imply its endorsement, recommendation, or favoring by the United States government or Lawrence Livermore National Security, LLC. The views and opinions of authors expressed herein do not necessarily state or reflect those of the United States government or Lawrence Livermore National Security, LLC, and shall not be used for advertising or product endorsement purposes.

Single Particle X-ray Diffractive Imaging

Michael J. Bogan,[1*] W. Henry Benner,[1] Sébastien Boutet,[1,2,3] Urs Rohner,[1] Matthias Frank,[1] Anton Barty,[1] Marvin Seibert,[3] Filipe Maia,[3] Stefano Marchesini,[1†] Saša Bajt,[1††] Bruce Woods,[1] Vincent Riot[1], Stefan P. Hau-Riege,[1] Martin Svenda,[3] Erik Marklund,[3] Eberhard Spiller,[4] Janos Hajdu,[2,3] and Henry N. Chapman[1,5]

1. Lawrence Livermore National Laboratory, 7000 East Avenue, Livermore CA 94550, USA.

2. Stanford Synchrotron Radiation Laboratory, Stanford Linear Accelerator Center, 2575 Sand Hill Road, Menlo Park, California 94305, USA.

3. Laboratory of Molecular Biophysics, Institute of Cell and Molecular Biology, Uppsala University, Husargatan 3, Box 596, S-75124 Uppsala, Sweden.

4. Spiller X-ray Optics, Livermore CA 94550, USA.

5. Centre for Free-Electron Laser Science, Universität Hamburg, Notkestraße 85, 22607 Hamburg, Germany.

Author email address: bogan2@llnl.gov

*Corresponding author: Michael J. Bogan, Applied Physics and Biophysics, Lawrence Livermore National Laboratory, 7000 East Avenue L-211, Livermore CA 94550, USA

Current Addresses: †Advanced Light Source, MS 2-400, Lawrence Berkeley National Laboratory, 1 Cyclotron Road, Berkeley, CA 94720, USA; ††Deutches Elektronen Synchrotron, Notkestraße 85, 22607 Hamburg, Germany.

Table of Contents Figure:
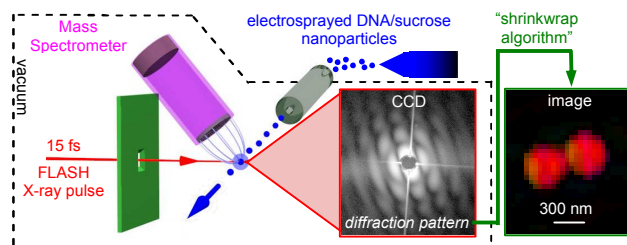
1   ABSTRACT: **In nanotechnology, strategies for the creation and manipulation of**
2   **nanoparticles in the gas phase are critically important for surface modification and**
3   **substrate-free characterization. Recent coherent diffractive imaging with intense**
4   **femtosecond X-ray pulses has verified the capability of single-shot imaging of**
5   **nanoscale objects at sub-optical resolutions beyond the radiation-induced damage**
6   **threshold. By intercepting electrospray-generated particles with a single 15**
7   **femtosecond soft-X-ray pulse, we demonstrate diffractive imaging of a nanoscale**
8   **specimen in free flight for the first time, an important step toward imaging**
9   **uncrystallized biomolecules.**

12   Development of methods enabling higher spatial and time resolution characterization of

13   nanoscale objects such as single particles and biomolecules is essential to achieve the

14   goals of nanotechnology and to push structural biology into new frontiers. We are

15   developing strategies to enable characterization of nanoscale objects using the first

16   operational soft X-ray free electron laser (FEL), the FLASH facility at DESY in

17   Hamburg, Germany.[1, 2] This facility produces ultrafast (<30 fs) and ultrabright coherent

18   X-ray pulses (peak brightness $>10^{30}$ photons/s/mrad^2/mm^2 /(0.1% bandwith), or $>10^{12}$

19   photons/pulse) and provides many new possibilities for probing nanoscale objects.[3]

20   Examples of new capabilities demonstrated at FLASH include femtosecond time-

21   resolved holography for measurements of nanoparticle dynamics[4] and single-pulse

22   diffractive imaging of nanostructured materials.[5] In diffractive imaging a sample is

23   illuminated by coherent X-rays, a far-field diffraction pattern is recorded on an area

24   detector, such as a CCD, and the image is reconstructed using iterative phase retrieval

25   algorithms.[6, 7] During initial experiments at FLASH, samples were mounted on

26   supporting silicon nitride membranes that contributed background scattering to the

27   measurements. When the number of atoms in the substrate becomes much larger than the

28   number of atoms in the sample itself, such as in the case of isolated biomolecules on a

29   membrane, this background is expected to dominate the signal measured by the CCD.

30   This motivates the development of sample handling systems free of supporting

membranes, such as particle beams, for introducing particles and biomolecules into the X-ray beam. Successful implementation of such container-free sampling methods may enable structural determinations without the need for a crystal.[8-10]

Particle beams have been at the vanguard of research in most branches of science. Recently, strategies for manipulating nanoparticles in the gas phase using their inertial properties are gaining interest in the manufacture of nanostructured materials[11, 12] and for substrate-free particle characterization *in vacuo*.[13-15] A key development in the generation of focused nanoparticle beams *in vacuo* was Liu *et al.*'s implementation of thin plate orifices to manipulate particle spatial distribution prior to them passing through a nozzle and subsequently undergoing supersonic expansion.[16, 17] An axisymmetric stack of these thin plate orifices, or aerodynamic lenses, provides successive contractions of a flowing particle beam and enables focusing of a wide range of particle sizes (1 nm to 10 μm).[18] In this letter we demonstrate a viable technique, based on such an aerodynamic lens stack, for introducing isolated single particles in free flight into a pulsed X-ray beam for substrate-free imaging. We demonstrate an imaging resolution of better than 40 nm by diffractive imaging with the single X-ray pulse, and further characterize the interaction by mass spectrometry.

Substrate-Free Particle Delivery to X-rays. Our experimental geometry (Figure 1) is based on that previously used to image samples on silicon nitride foils.[5] Pulses from the FLASH FEL are condensed to a 20-μm diameter beam at the sample plane using a grazing-incidence ellipsoidal mirror. No monochromator or pinhole is used to limit the beam since the FEL output has sufficient temporal and spatial coherence for diffractive imaging. Instead of micro-positioning a substrate-supported sample into the beam, the apparatus is designed to introduce a continuous particle beam transmitted by an aerodynamic lens stack into the FEL beam. To steer the particle beam to intersect with the X-ray beam, the aerodynamic lens stack is mechanically translated. This is achieved by translating the entire differential pumping interface, represented in Fig. 1 (iv), in which the lens stack is integrated

1   The sample is generated using a charge-reduced nanoelectrospray aerosol source.[19] The
2   method is well characterized, has previously been used to prepare samples of spherical
3   nanoparticles on silicon nitride foils for characterization at FLASH,[20] and is applicable to
4   a wide variety of nanoscale materials that are likely to be characterized using FELs
5   including carbon nanotubes,[21] large biomolecules,[22] viruses[23-25] and cells.[26] One
6   particular sample of interest is scaffolded DNA origami, consisting of double-stranded
7   DNA programmed to form predefined two-dimensional geometrical shapes.[27] We are
8   investigating DNA nanostructures because they may be useful as nano-breadboards for
9   the arrangement of nano-objects or biomolecules for enhancing the signal-to-noise ratio
10 in single particle imaging methods, including holography with a complicated reference.[28]
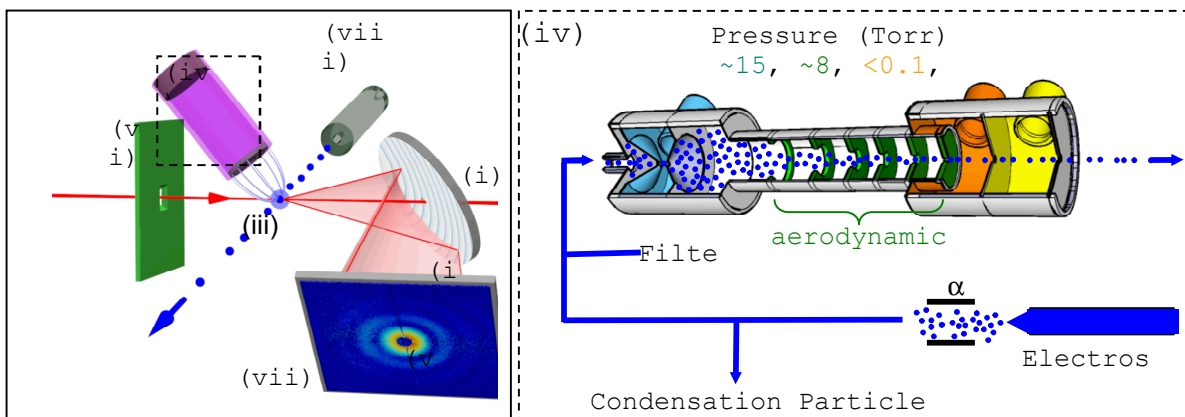
11 **Figure 1.** Schematic diagram of the experimental apparatus (not to scale). The FEL
12 pulses (i) are incident from the right, pass through an aperture designed to block stray
13 light (ii) and are focused to a 20 μm spot that defines the interaction region (iii).
14 Electrospray-generated aerosol is charge-neutralized via an α source and delivered into
15 vacuum through a differential pumping interface equipped with an aerodynamic focusing
16 system (iv). The pressure in the three pumping regions, coloured blue, orange and yellow,
17 are set to optimize the focusing of the nanoparticles through an aerodynamic lens stack
18 (green). The resultant continuous stream of nanoparticles travels at ~150 m/s and is
19 confined to a beam of ~250-μm diameter (v). The nanoparticles are steered into the
20 interaction region using mechanical translation of the entire differential pumping
21 interface. X-rays diffracted from the interception of single nanoparticles by the FEL
22 reflect from a graded multilayer planar mirror (vi) to the single photon sensitive X-ray
23 CCD (vii) while the direct beam passes through a hole in the centre of the mirror. Ions
24 created from the FEL interactions are detected by a miniature time-of-flight mass
25 spectrometer (viii).

26

27

1   For the first experiments it was essential to use particles that would produce strong

2   diffraction patterns. When electrosprayed, individual megadalton DNA complexes have

3   an aerodynamic diameter of 28 nm (Figure 2). The X-ray intensity produced by focusing

4   the beam to a diameter of 20-µm was not sufficient to record single pulse diffraction

5   patterns of these particles. We increased the signal by enlarging the particles to increase

6   their scattering cross section. Larger particles were created using Kaufman's *in-situ*

7   electrospray method for synthesis of sucrose encapsulated biomolecules.[29] Sucrose is

8   added to the starting solution and upon evaporation of the dilute ammonium acetate/water

9   buffer, sucrose-encapsulated DNA is created. The diameter of the composite nanoparticle

10   is given by $[d_m^3 + d_{suc}^3]^{1/3}$, where d_m and d_{suc} are the diameters of the discrete

11   macromolecule (28 nm for the DNA complexes) and residue particles of sucrose (80 nm)

12   when electrosprayed separately.[29] The composite sucrose/DNA particles averaged 81 nm

13   in diameter and their mass is dominated by the sucrose (Figure 2). Particles larger or

14   smaller than 81 nm resulted from variations in the initial volume of droplets emitted and

15   from periodic instability of the electrospray source. All particle sizes are directed toward

16   the FEL.
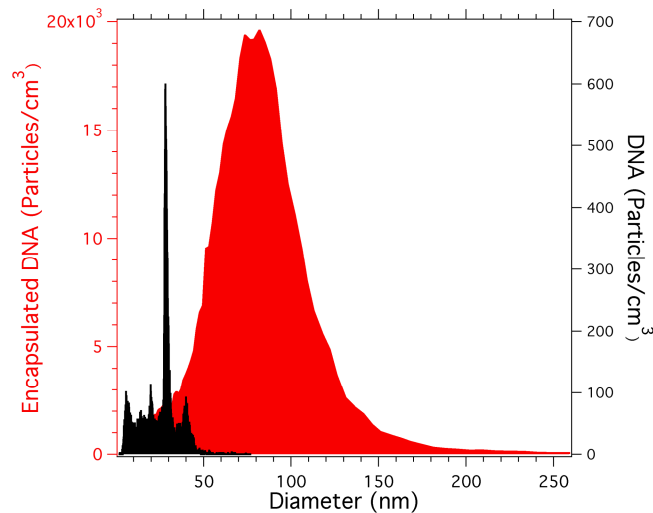
17   **Figure 2.** Size distribution of scaffolded DNA electrosprayed from a 25 mM
18   ammonium acetate solution containing 0% (black) and 50 % (red) sucrose, as measured
19   by scanning mobility particle size spectrometry. Both bare DNA and sucrose-
20   encapsulated DNA were injected into the FEL beam.

21

22
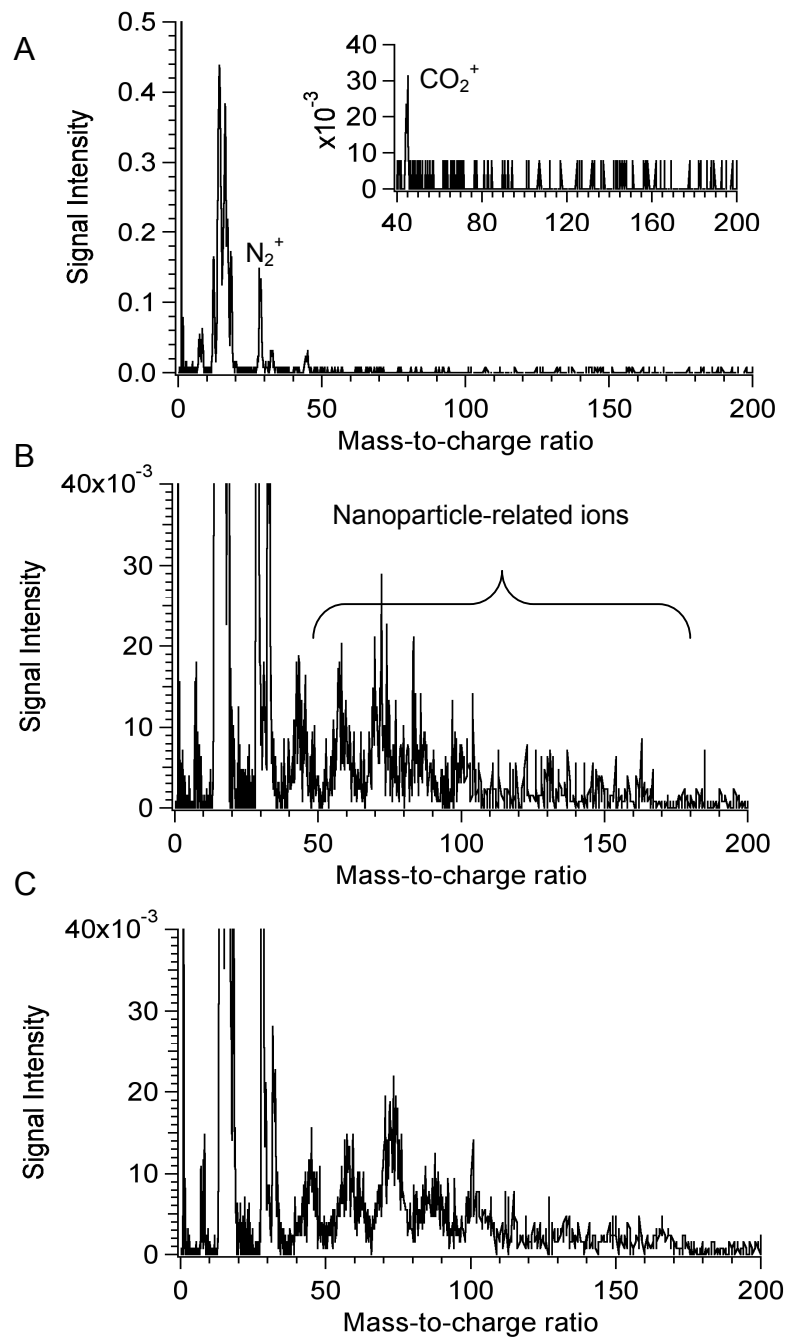
Figure 3. Time-of-flight mass spectra of ions created by a single FEL pulse from (A) background gas, (B) the single particle hit in Fig. 4A and (C) the particles hit in Fig. 4B.

Mass Spectrometry. Individual particles are intercepted by the FEL randomly, therefore a time-of-flight mass spectrometer (TOFMS) is used to identify particle interception events. Mass spectra can be collected at a rate of 100 kHz. Gases delivered through the injector to the interaction region (primarily N_2, O_2 and CO_2) were ionized by the FEL,

1   resulting in TOFMS detection of the ions N^{2+}, N^+, O^{2+}, O^+, OH^+, H_2O^+, N_2^+, O_2^+, and

2   CO_2^+ (Figure 3A). Particle interception events produced ions with mass-to-charge ratios

3   greater than 50 (Figure 3B). These ions are consistent with the ions created from sucrose

4   particles in other high temperature ion sources, such as inductively coupled plasma (7000

5   K).[30] In this case the particle is heated to ~60000 K during the interaction[5] and the

6   mechanism of ion generation has not been elucidated. These are the first mass spectra

7   ever collected from biological materials ionized by a soft X-ray FEL.

8

9   **Single Particle Imaging.** X-rays diffracted from material in the interaction region reflect

10   from a graded-period multilayer-coated mirror to a single photon sensitive X-ray CCD

11   while the direct beam passes through a hole in the center of the mirror. For these

12   experiments FLASH was operated in multi-bunch ultrashort pulse mode[1] to increase the

13   rate of particle interception. Pulse bunches were delivered at 5 Hz and each bunch

14   consisted of 27 X-ray pulses separated by 10 μs. Each pulse was transform limited and

15   typically dominated by a single mode, i.e. it had almost complete transverse and

16   longitudinal coherence. This high degree of coherence is a requirement for high-

17   resolution imaging and results in the ability to utilize essentially the entire output of the

18   source for our experiments. The mean photon wavelength was 13.5 nm, the average pulse

19   energy was about 20 μJ, equivalent to about 1.4×10^{12} photons, and the pulse duration

20   was 15 ± 5 fs.

21   The diffraction pattern recorded by a typical CCD readout when the FEL intercepts a

22   particle is shown in Figure 4A. The strong near vertical and horizontal lines that pass

23   through the center of the pattern are caused by the 200 μm square window aperture

24   (Figure 1, (ii)). This aperture is used to block scattered light from the ellipsoidal mirror

25   which would otherwise add noise to the diffraction pattern. We find that a square

26   aperture produces secondary scattering that is localized in the diffraction pattern and

27   which can be easily filtered from the pattern, whereas a circular aperture distributes

28   secondary scattering across the entire pattern. The dark area on the left of the pattern is a

29   shadow due to the mass spectrometer and the vertical line on the right of the pattern is

30   due to a column defect in the CCD.
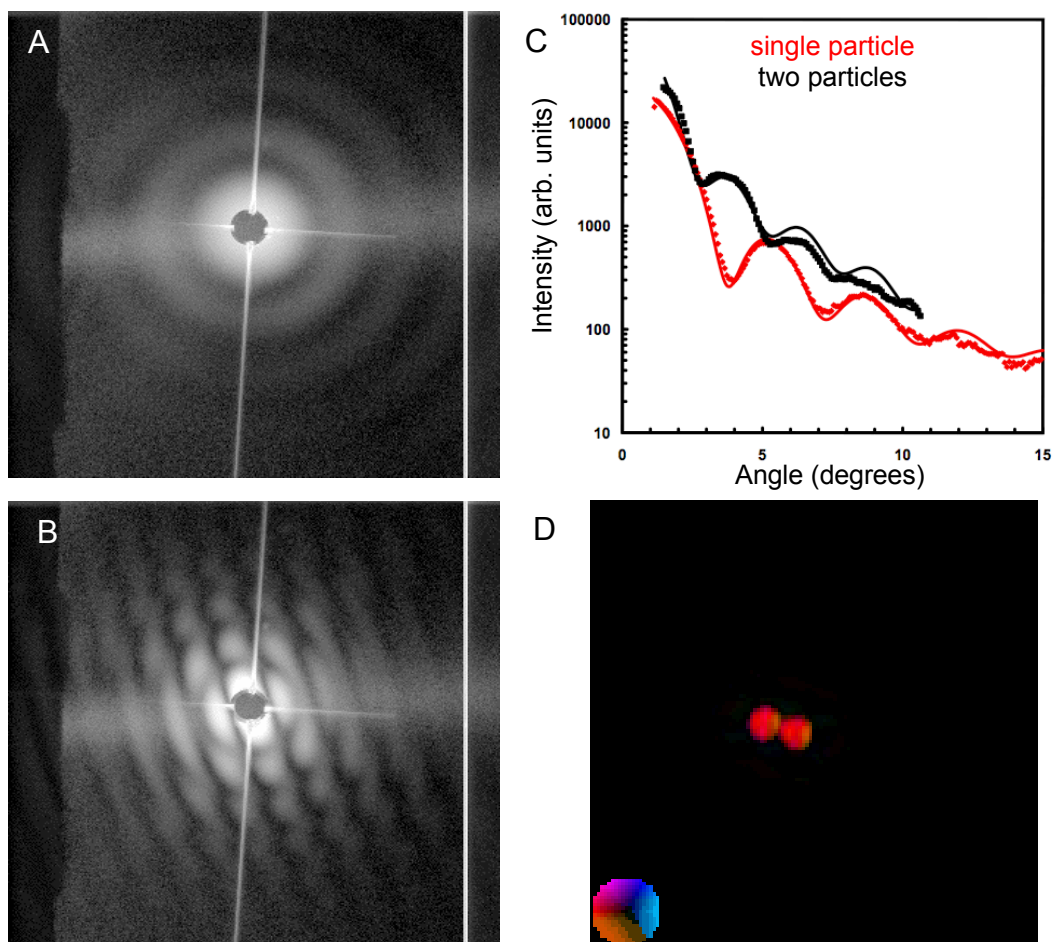
Figure 4. FLASH X-ray coherent diffraction patterns of (A) a single particle and (B) two particles. The intensity is shown on a logarithmic grey scale with black denoting 1 photon/pixel and white denoting 16500 photons/pixel. Each diffraction pattern is integrated over 243 FEL pulses, one of which intercepted the particles. The entire pattern as detected by the CCD is shown. (C) Radial averages of the angle-resolved signal intensity for the single particle from (A) and the two particles from (B). The markers are experimental data and the solid lines are calculated with Mie theory, which predicts diameters of 248 ± 10 nm and 330 ± 20 nm (assuming identical size for the pair) respectively. (D) The X-ray image reconstructed from data in (B) shows that the two particles, each ~325 nm in diameter, are in contact. Pixel size in the reconstruction is 30.3 nm and the hue denotes the phase of the solution as in the color wheel.

This diffraction pattern exhibits the characteristic Airy rings of a spherical particle, indicating that a spherical residue particle is created as the solvent evaporates from the electrospray droplet and the sucrose encapsulates the DNA. The particle diameter (248 ±

1   10 nm) was determined by fitting the radial average of the signal intensity to Mie theory

2   (Figure 4B). The strategy of encasing material in sucrose has the potential to be refined to

3   create molecular tampers predicted to delay the onset of damage to biomolecules during

4   intense single pulse X-ray exposures.[31]

5

6   Several diffraction patterns indicative of two particles being intercepted by a single FEL

7   pulse simultaneously were also captured unexpectedly (Figure 4C). The diffraction

8   pattern shows fringes due to interference between the scattered waves from two particles.

9   This coherent addition would not be present if two particles are hit by two different

10   pulses. Mass spectrometer data collected for each individual FEL pulse during the CCD

11   acquisition verified that only a single particle interception event occurred, producing the

12   mass spectrum in Figure 3C. The well-defined Airy ring pattern in Figure 4C suggests

13   that the two particles hit by the same pulse are of similar diameter, calculated to be $330 \pm$

14   20 nm (Figure 4B). The deviation from the Mie theory is attributed to the low signal-to-

15   noise ratio of the diffraction pattern at high angles and the assumption that both particles

16   are of identical diameter. The two minima in the central ring suggest that the distance

17   between the balls in the direction transverse to the beam is the same as their size, i.e. the

18   two particles are in contact and constitute a single dimer particle (see supplemental

19   information). Such a particle could have been created through agglomeration during

20   transport or from two DNA complexes being present in a larger droplet.

21   Real-space images of nanoscale objects can be obtained from single pulse coherent

22   diffraction patterns using iterative projection algorithms for phase retrieval.[5, 7] A

23   reconstructed image of the two-particle pattern reveals that the two particles were in

24   contact, forming a dimer (Figure 4D). The resolution of this image is 40 nm. Each

25   particle was 325 nm in diameter, corresponding to the Mie calculated diameter. This is

26   the first image of a substrate-free individual nanoparticle reconstructed from a diffraction

27   pattern created by a single FEL pulse and represents the first step toward imaging of

28   single biomolecules using future X-ray FELs.

29

30   **Single Particle Image Acquisition Rate.** Over the length of a 2.5 hour experiment, a

31   total of 105 particle diffraction patterns were recorded. The average rate was 0.012

1 particle diffraction patterns collected per second or approximately 1 per minute (Figure

2 5A, solid square). The expected rate of image collection for this single particle diffractive

3 imaging technique can be calculated using a modification of an equation derived by Kane

4 *et al.*[32, 33] for determining aerosol mass spectrometry hit rates (HR),

5
$$HR = nVTf\left(\frac{r_L^2 h}{r_P^2 v}\right) \tag{1}$$

6 where n is the aerosol number density, V is the volume flow of aerosol through the inlet,

7 T is the inlet transmission efficiency, h is the X-ray laser beam height (width along the

8 particle beam axis), v is the particle velocity and r_L and r_P are the radius of the FEL pulse

9 and the particle beam, respectively. The fixed repetition rate, f, of FLASH and the

10 random arrival of particles transmitted through the aerodynamic lens results in hits

11 occurring only when there is coincidental overlap of individual particles with the pulsed

12 laser.

13

14 Encapsulated DNA nanoparticles were prepared as an aerosol with a concentration of n

15 $= 3 \times 10^4$ particles/cm^3, were sampled by the aerodynamic lens inlet at a rate of $V = 14.33$

16 cm^3/second and traveled through the interaction region at $v = 150$ m/s. FEL pulses were

17 delivered at $f = 135$ pulses/second. The interaction volume (Figure 1, point (iii)) is

18 defined by the particle beam diameter ($2r_P = 250$ µm) and the FEL focus ($2r_L = 20$ µm in

19 diameter). Using these parameters Eqn. (1) predicts a hit rate of 0.06 particles/second,

20 assuming a transmission efficiency of $T = 10$ percent and setting h equal to the particle

21 beam diameter (Figure 5A). The average hit rate (0.07 particles/second) over a 200

22 second period of our experiment agreed with the predicted hit rate (Figure 5B). The

23 discrepancy between the predicted and measured value over the longer experiment is in

24 part due to steering of the particle beam and down time when changing between pure

25 sucrose and sucrose/DNA samples. We note that the hit rate increases linearly with laser

26 repetition rate, so without modification of our experimental apparatus the hit rate will

27 improve as the FEL pulse rate increases: FLASH has recently been operated at 700

28 pulses/second with design specifications of over 1500 pulses/second,[2] giving an

29 immediate factor of between 5 to 11 increase in hit rate.

1

2
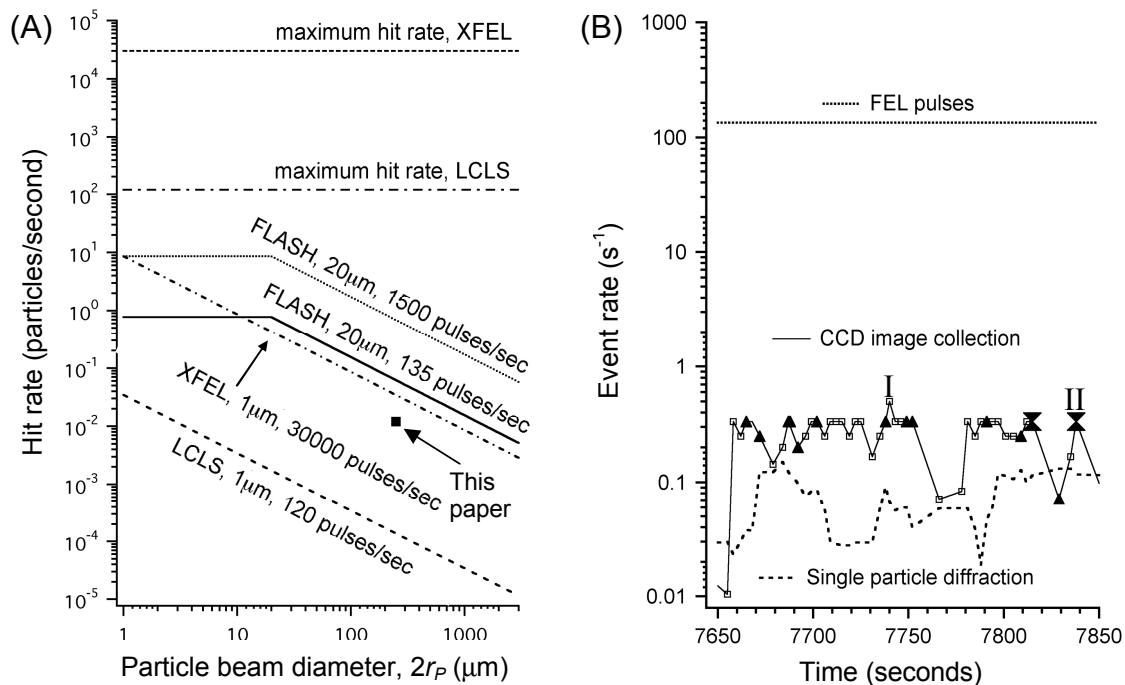
Figure 5. (A) Predicted hit rates at FLASH, XFEL and LCLS of nanoparticles, electrosprayed to an aerosol concentration of 3×10^4 particles/cm^3, for varying particle beam diameter. The maximum hit rate is equal to the maximum number of pulses per second from the FEL. Annotation denotes X-ray source, FEL beam diameter, and number of pulses delivered per second. The filled square is the average hit rate measured at FLASH during a 2.5 hour experiment with 135 FEL pulses/second. (B) Comparison of the rates of FEL pulse (and mass spectrometer acquisition), CCD image acquisition and single particle diffraction events over a 200 second period of a single particle diffractive imaging experiment. Markers on CCD line: open square = no particle hit, triangle = single particle hit, double triangle = dimer particle hit. Diffraction patterns collected at CCD readouts I, and II are shown in Figure 4.

Discussion. Experiments at future hard-X-ray FELs, such as the Linac Coherent Light Source (LCLS) and the European X-ray Laser (XFEL), are predicted to enable the determination of three-dimensional biomolecular structure at near-atomic resolution without crystallization. Such an experiment is currently predicted to require $>10^4$ images of identical biomolecules,[8, 9] thus maximizing the hit rate achievable by single particle imaging is critical to reduce the data acquisition time. Further exacerbating the challenge

11

is that the X-ray beam must be focused down to much smaller spot sizes, typically below 1 μm, to increase the incident intensity and ensure adequate signal at the higher photon momentum transfers (higher resolutions) that the shorter wavelength affords. This will immediately decrease the efficiency of the apparatus demonstrated here by a factor of 400 or more based on the 20 μm diameter FEL beam at FLASH.

FEL laser repetition rate is another critical factor. At the European XFEL the inefficiencies due to FEL beam size will be made up by the increased FEL pulse rate of up to 30,000 pulses/second. For a source aerosol concentration of 3×10^4 particles/cm^3, this results in an expected hit rate that is only half of that measured at FLASH during the experiments reported in this letter. Hit rates at LCLS may be significantly lower because the planned pulse rate is 120 pulses/second. We summarize the potential hit rates at FLASH and future FEL facilities in Fig. 5A, considering only FEL machine parameters and assuming no further improvements in aerodynamic focusing or aerosol density. This is therefore a pessimistic estimate assuming no further sample handling development.

Image acquisition rates will be improved in a number of ways independent of the X-ray source used. For example, improved particle beam focusing to match the sub-micron FEL beam size may be possible through developments in the aerodynamic lens stack itself. If the exit nozzle of the aerodynamic lens stack is positioned in closer proximity to the interaction region, the effect of the divergence angle (currently 0.5 to 3 degrees) of the particle beam imparted by gas expansion will be reduced. It may also be possible to increase the particle density sampled by the aerosol handling system using multi-nozzle electrospray or droplet sources.[34, 35]

A key advantage of using aerodynamic focusing for single particle X-ray diffractive imaging is that it is a leak in the vacuum chamber that continuously samples from atmospheric pressure (at a rate of 14.33 cm^3 s^{-1} for the current design). Thus any aerosol existing near the inlet is passively sampled. This enables us to utilize the advantages of well-characterized atmospheric aerosol sources such as electrospray for preparing samples to be imaged. Many other atmospheric pressure aerosolization methods,

including flames, atomizers, and lasers, can also be used. All of these aerosol sources can be interchanged instantaneously or operated simultaneously. Many of these aerosol sources can generate particle concentrations equivalent to or greater than the $3x10^4$ particles/cm^3 used here. Each type of source generates particles and size distributions with unique characteristics that make them more or less applicable to the nanoscale biomaterials we studied by electrospray. For example, aerosol sources used in atomic cluster research often operate at concentrations of 10^{10} clusters/cm^3 and will certainly be a useful source for single particle X-ray diffractive imaging of core-shell structured atomic clusters. However, they are currently not suitable for biomolecule imaging. To put these aerosol concentrations into a real-world perspective, measurements of the aerosol concentration generated by automobiles near highways show a total of 10^4-10^6 particles/cm^3,[36] suggesting it may even be possible to image environmental particles.

Another advantage of aerodynamic lens interface is its ability to continuously operate for many hours without clogging, a crucial characteristic for successful utilization of precious X-ray FEL beam time. The key limitation of this method is the current inability to time arrival of particles with the FEL pulses. Single particle sources designed to deliver proteins in synchronization with the X-ray pulses are also being developed[37] and, if successful, may overcome the inefficiency of operation in free-fire mode. It is anticipated that continued development of single particle sources of all types will increase the number of accessible sample types and raise the achievable hit rate to the maximum levels available for both LCLS and XFEL. Detectors designed to accommodate single particle diffraction data acquisition at such high rates are in development.

The ultimate goal for single molecule X-ray imaging is the delivery of a sufficient number of identical molecules to enable 3D reconstruction. Any diffraction patterns of non-identical molecules collected will reduce the effective hit rate and increase the complexity of classifying images of molecules in different orientations. Future experiments will make use of particle size selection technology such as differential mobility methods.[20] This approach can be used to remove contaminants such as residue particles or to select molecular conformations, potentially reducing the complexity of

1 classifying diffraction patterns. Also note that the thickness of the sucrose coatings,

2 which in our experiments had a broad distribution, can currently be controlled to less than

3 1 nm.[29]

4

5   The resolution obtained in single pulse X-ray imaging experiments is limited in part by

6 the onset of damage in the sample due to the intense X-ray pulse. Depending on the pulse

7 duration, the resolution limit may be 0.5 nm for hard-X-ray FEL pulses, or even less with

8 encapsulated particles.[31] For the pulse fluences and wavelength of these experiments,

9 calculations show that the diffraction pattern formed by the pulse would be essentially the

10 same as the undamaged case and that any expansion of the particle would certainly be

11 much less than the resolution length of 40 nm.[38] Furthermore, diffractive imaging of well

12 characterized nano-structured objects at FLASH, at 32-nm wavelength, have shown no

13 measurable damage.[5] In the experiments reported here we are not able to probe the

14 extent of damage in the sample due to unknown shape and size characteristics of the

15 individual sucrose-encapsulated DNA particles imaged during a specific pulse. Future

16 work investigating the onset of damage in particles in free flight will utilize size-

17 monodisperse spherical nanoparticles that have been diameter-selected by differential

18 mobility methods[20] and sampled directly into the aerodynamic lens stack. This approach

19 will be an extension of our method for measuring X-ray pulse-induced damage at

20 femtosecond time resolutions with size-selected spherical nanoparticles deposited onto

21 silicon nitride membranes.[4]

22

23   Our results unequivocally show the feasibility of single-particle X-ray diffractive

24 imaging using FELs. It is expected that future X-ray FEL facilities will enable nanometer

25 to atomic scale resolution imaging of non-crystalline nanoscale materials, such as large

26 biomolecules, viruses or cells, inorganic particles and environmental particles. Single

27 particle X-ray diffractive imaging will provide new capabilities for following the

28 dynamics of materials at the atomic time and length scales, potentially resulting in

29 significant advances in nanotechnology development and structural biology.

30

21

22 REFERENCES:

23 1. Ayvazyan, V.; Baboi, N.; Bahr, J.; Balandin, V.; Beutner, B., *et al. Eur. J. Phys. D*
24   **2006,** 37, 297-303.
25 2. Ackermann W.; Asova G.; Ayvazyan V.; Azima A.; Baboi N., *et al. Nat. Photon.*
26   **2007,** 1, (6), 336-342.
27 3. Gaffney, K. J.; Chapman, H. N. *Science* **2007,** 316, (5830), 1444-1448.
28 4. Chapman, H. N.; Hau-Riege, S. P.; Bogan, M. J.; Bajt, S.; Barty, A., *et al. Nature*
29   **2007,** 448, (9), 676-679.
30 5. Chapman, H. N.; Barty, A.; Bogan, M. J.; Boutet, S.; Frank, M., *et al. Nat. Phys.*
31   **2006,** 2, (12), 839-843.
32 6. Fienup, J. R. *Appl. Opt.* **1982,** 21, 2758-2769.
33 7. Marchesini, S. *Rev. Sci. Instr.* **2007,** 78, (4), 011301.
34 8. Neutze, R.; Wouts, R.; van der Spoel, D.; Weckert, E.; Hajdu, J. *Nature* **2000,** 406,
35   752-757.

9. Huldt, G.; Szoke, A.; Hajdu, J. *J. Struct. Biol.* **2003,** 144, 219-227.

10. Spence, J. C. H.; Doak, B. *Phys. Rev. Lett.* **2004,** 92, 198102.

11. Piseri, P.; Tafreshi, H. V.; Milani, P. *Curr. Op. Solid State Mater. Sci.* **2004,** 8, (3-4), 195-202.

12. Carbone, R.; Giorgetti, L.; Zanardi, A.; Marangi, I.; Chierici, E., et al. *Biomaterials* **2007,** 28, (13), 2244-2253.

13. Noble, C. A.; Prather, K. A. *Mass Spectrom. Rev.* **2000,** 19, 248-274.

14. Wilson, K. R.; Peterka, D. S.; Jimenez-Cruz, M.; Leone, S. R.; Ahmed, M. *Phys. Chem. Chem. Phys.* **2006,** 8, (16), 1884-1890.

15. Shu, J.; Wilson, K.; Ahmed, M.; Leone, S. R. *J. Chem. Phys.* **2006,** 124, 034707.

16. Liu, P.; Ziemann, P. J.; Kittleson, D. B.; McMurry, P. H. *Aerosol Sci. Tech.* **1995,** 22, 314-324.

17. Liu, P.; Ziemann, P. J.; Kittleson, D. B.; McMurry, P. H. *Aerosol Sci. Tech.* **1995,** 22, 293-313.

18. Wexler, A. S.; Johnston, M. V., Real-time single-particle analysis. In *Aerosol Measurement*, Baron, P. A.; Willeke, K., Eds. John Wiley & Sons: Hoboken, New Jersey, 2005; pp 365-386.

19. Chen, D. R.; Pui, D. Y. H.; Kaufman, S. L. *J. Aerosol Sci.* **1995,** 26, (6), 963-977.

20. Bogan, M. J.; Benner, W. H.; Hau-Riege, S. P.; Chapman, H. N.; Frank, M. *J. Aerosol Sci.* **2007,** 38, (11), 1119-1128.

21. O'Shea, J. N.; Taylor, J. B.; Swarbrick, J. C.; Magnano, G.; Mayor, L. C., et al. *Nanotechnology* **2007,** 18, (3), 035707.

22. Bacher, G.; Szymanski, W. W.; Kaufman, S. L.; Zollner, P.; Blaas, D., et al. *J. Mass Spectrom.* **2001,** 36, 1038-1052.

23. Hogan, C. J. J.; Kettleson, E. M.; Ramaswami, B.; Chen, D. R.; Biswas, P. *Anal. Chem.* **2006,** 78, (3), 844-852.

24. Bothner, B.; Siuzdak, G. *ChemBioChem* **2004,** 5, 258-260.

25. Tito, M. A.; Tars, K.; Valegard, K.; Hajdu, J.; Robinson, C. V. *J. Amer. Chem. Soc.* **2000,** 122, (14), 3550-3551.

26. Blades, A. T.; Ikonomou, M. G.; Kebarle, P. *Anal. Chem* **1991,** 63, (19), 2109-2114.

27. Rothemund, P. W. K. *Nature* **2006,** 440, 297-302.

28. Hau-Riege, S. P.; Szoke, H.; Chapman, H. N.; Szoke, A.; Marchesini, S., *et al. Acta Crystallographica Section A* **2004,** 60, (4), 294-305.

29. Kaufman, S. L. *Anal. Chim. Acta* **2000,** 406, (1), 3-10.

30. Taylor, V. F.; March, R. E.; Longerich, H. P.; Stadey, C. J. *Int. J. Mass Spectrom.* **2005,** 243, (1), 71-84.

31. Hau-Riege, S. P.; London, R. A.; Chapman, H. N.; Szoke, A.; Timneanu, N. *Phys. Rev. Lett.* **2007,** 98, 198302.

32. Kane, D. B.; Johnston, M. V. *Environ. Sci. Technol.* **2000,** 34, 4887-4893.

33. Kane, D. B.; Oktem, B.; Johnston, M. V. *Aerosol Sci. Tech.* **2001,** 34, (6), 520 - 527.

34. Deng, W.; Klemic, J. F.; Li, X.; Reed, M. A.; Gomez, A. *J. Aerosol Sci.* **2006,** 37, 696-714.

35. Bocanegra, R.; Galan, D.; Marquez, M.; Loscertales, I. G.; Barrero, A. *J. Aerosol Sci.* **2005,** 36, 1387-1399.

36. Kittelson, D. B.; Watts, W. F.; Johnson, J. P.; Remerowki, M. L.; Ische, E. E., *et al. Inhalation Toxicology* **2004,** 16, (11 supp 1), 31 - 39.

1   37. Weierstall, U.; Doak, R. B.; Spence, J. C. H.; Starodub, D.; Shapiro, D., *et al. Exp.*
2   *Fluids* **2007,** in press.
3   38. Hau-Riege, S. P.; London, R. A.; Bergh, M.; Chapman, H. N. *Phys. Rev. E* **2007,** 76,
4   046403.
5
6